Origins of Deuterium Kinetic Isotope Effects on the Proton Transfers of the Bacteriorhodopsin Photocycle†

Leonid S. Brown,‡ Richard Needleman,§ and Janos K. Lanyi*,‡

Department of Physiology and Biophysics, University of California, Irvine, California 92697, and Department of Biochemistry, Wayne State University, Detroit, Michigan 48201

Received September 21, 1999; Revised Manuscript Received November 10, 1999

ABSTRACT: Deuterium kinetic isotope effects (KIE) were measured, and proton inventory plots were constructed, for the rates of reactions in the photocycles of wild-type bacteriorhodopsin and several site-specific mutants. Consistent with earlier reports from many groups, very large KIEs were observed for the third (and largest) rise component for the M state and for the decay of the O state, processes both linked to proton transfers in the extracellular region. The proton inventory plots (ratio of reaction rates in mixtures of H_2O and D_2O to that in H_2O vs mole fraction of D_2O) were approximately linear for the first and second M rise components and for M decay, as well as for O decay, indicating that the rates of these reactions are limited by simple proton transfer. Uniquely, the third rise component of M (and in the D96N mutant also a fourth rise component) exhibited a strongly curved proton inventory plot, suggesting that its rate, which largely accounts for the rate of deprotonation of the retinal Schiff base, depends on a complex multiproton process. This curvature is observed also in the E194Q, E204Q, and Y57F mutants but not in the R82A mutant. From these findings, and from the locations of bound water in the extracellular region in the crystal structure of the protein [Luecke, Schobert, Richter, Cartailler, and Lanyi (1999) *J. Mol. Biol. 291,* 899−911], we suspect that the effects of deuterium substitution on the formation of the M state originate from cooperative rearrangements of the extensively hydrogen-bonded water molecules 401, 402, and 406 near Asp-85 and Arg-82.

The reaction cycle ("photocycle") of the light-driven transport of protons in bacteriorhodopsin includes direct proton transfers between neighboring donors and acceptors within the protein, protonation/deprotonation reactions dependent on long-range interactions between protonatable groups, and proton release and uptake at the aqueous membrane interfaces (*1*−*4*). In the L to M_1 reaction of the photocycle the changed pK_a's of donor and acceptor result in the development of a protonation equilibrium between the Schiff base of the photoisomerized 13-*cis*,15-*anti*-retinal and Asp-85. Protonation of Asp-85 causes release of a proton to the extracellular surface, and the coupling of this release to the pK_a of Asp-85 (*5*−*7*), as well as what may be a protein conformation change in the kinetic step described as the M_1 to M_2 reaction (*8, 9*), shifts the protonation equilibrium toward complete deprotonation of the Schiff base. In the M_2 to N reaction the Schiff base is reprotonated by Asp-96, and during the N to O reaction Asp-96 is protonated from the cytoplasmic surface. In the final step, the BR state recovers through proton transfer from Asp-85 to the extracellular proton release site (*10, 11*).

The spectral changes during the photocycle are more complex than expected from this simple sequence, and this complexity has been explained by various schemes, including some with equilibration reactions (*12*−*15*) and others with branched unidirectional reactions or multiple bacteriorhodopsin populations (*16*−*18*). Although the observable relaxation times are complex functions of the actual rate constants of the reactions and dependent on the kinetic model, in a linear sequence they do reflect the distinct molecular steps in the transport cycle listed above, i.e., the shifts of protonation equilibria, the retinal isomerization, etc. With this in mind, it had been noted in many earlier reports that the magnitudes of deuterium kinetic isotope effects (KIE)[1] were quite different for the different relaxations. Unusually large (5−10×) KIEs were observed for the component of the formation of M with greatest amplitude (*19*−*22*), assigned in one scheme to an "M_1 to M_2" reaction (*8, 12*) and in another to the L to M_1 reaction (*22*), and for the decay of the O state (*10, 19, 22, 23*). All other relaxations of the photocycle, including the decay of the M state, exhibited smaller (1−3×) KIEs. On this basis, it was suggested (*22*) that the proton transfers in the extracellular region occur by "ice-like" conduction, while those in the cytoplasmic region utilize conduction more like that in liquid water.

Recently, the structure of bacteriorhodopsin was determined by X-ray diffraction to resolutions high enough to

† This work was funded partly by grants from the National Institutes of Health (GM 29498 to J.K.L.), the Department of Energy (DEFG03-86ER13525 to J.K.L.), and the U.S. Army Research Office (DAAL03-92-G-0406 to R.N.).

* Correspondence should be addressed to this author. E-mail: jlanyi@orion.oac.uci.edu.

‡ University of California.

§ Wayne State University.

[1] Abbreviation: KIE, kinetic isotope effect (in this report it refers to the ratio of relaxation rates in 100% H_2O and 100% D_2O).

10.1021/bi9921900 CCC: $19.00
Published on Web 01/08/2000

identify the locations of bound water molecules and their hydrogen bonds (*24, 25*). The extracellular region was found to contain an extensive hydrogen-bonded network that connects the Schiff base, numerous ionizable residues, and many bound water molecules. The changes in this network, and the displacement of the side chain of Arg-82 toward the extracellular surface, detected in the crystal structure of the M state (*26*), must be the basis for the coupling that links the protonation of Asp-85 at one end of this network to the release of a proton to the surface at the other (*5*−*7*). The extracellular network must provide the means also for the movement of the proton from Asp-85 to the proton release site during decay of the O state at the end of the photocycle. Thus, the conclusions drawn from kinetics and deuterium KIEs need to be reexamined in light of the specific structural information now available. We report here on our attempt to do this.

Deuterium isotope effects in enzymes can be investigated in detail by the proton inventory method (*27*). The observed effects of deuterium substitution, e.g., on the rates or rate constants of the reactions, are plotted vs the mole fraction of D_2O. Simple hydrogen or proton transfer reactions yield straight lines, but more complex reactions yield curved lines. While there are numerous possible reasons for a curvature, for protonation reactions in proteins many of these complications are absent (*27*). In such systems there is no isotope fractionation in the stable states, i.e., deuterons and protons bind about equally at proton-binding sites, and the isotope effect is therefore ascribed to fractionation in the transition state. In such cases, curved proton inventory plots of the rate constants indicate cooperative interaction in the rate-limiting step. Numerous examples of such cases, for enzyme reactions of various kinds, are given in a detailed review of the method (*27*). More relevant for bacteriorhodopsin, according to recent results linear and curved proton inventory plots could distinguish between different rate-limiting processes for the last proton transfer in the transport cycles of cytochrome *c* oxidase in different species.[2]

MATERIALS AND METHODS

Purple membranes were prepared from *Halobacterium salinarum* by a standard method (*28*). The E194Q, E204Q, Y57F, R82A, and D96N mutants were constructed as described before (*29*) and isolated after expression in *H. salinarium* as purple membrane patches.

Kinetic measurements after photoexcitation with nanosecond laser flash at 420 and 660 nm were done as described earlier (*30*), using purple membranes suspended in mixtures of H_2O and D_2O and equilibrated overnight. For more details, and for proton kinetics with fluorescein covalently linked to Lys-129, see ref *21*. The pD in D_2O was taken as the apparent (measured) pH + 0.41 (*31*), scaled linearly in mixtures of D_2O and H_2O. Conditions were selected where pH (or pD) did not affect the rates to be determined. All measurements were at 15 °C.

RESULTS

Deuterium Isotope Effects in the Wild-Type Protein. Absorption changes at 420 nm in the photocycle originate mostly from the formation and decay of the M state, and their kinetics reveal the rate of the deprotonation and reprotonation of the retinal Schiff base, respectively. In Figure 1, traces of absorption rise and decay after flash excitation of wild-type bacteriorhodopsin are shown at different D_2O/H_2O ratios. The data could be fitted satisfactorily with three rise and one decay components (Table 1); this is illustrated by the absence of systematic features in the residual of the fit to one of the traces (Figure 1, lower panel). The first rise component had a relaxation time of 3 μs. Because of its small amplitude (in all cases but one, see below), but even more because the difference in the spectra of the K and L states at this wavelength contributes significantly to it (*32*), this phase will not be discussed. The relaxation rates of the second and third rise components, as well as the single decay component, exhibited characteristic deuterium isotope effects (Figure 2, Table 1). The amplitudes changed much less than the time constants with D_2O substitution (not shown), and this made the analysis of the data, as sums of exponentials, straightforward. The KIEs of these reactions were 1.8, 2.8, and 5.1, respectively (Table 1). The proton inventory plots for the single M decay component and the second and third M rise components were linear, somewhat curved, and greatly curved,[3] respectively (Figure 2). Under the conditions used, the O state did not accumulate significantly in this sample.

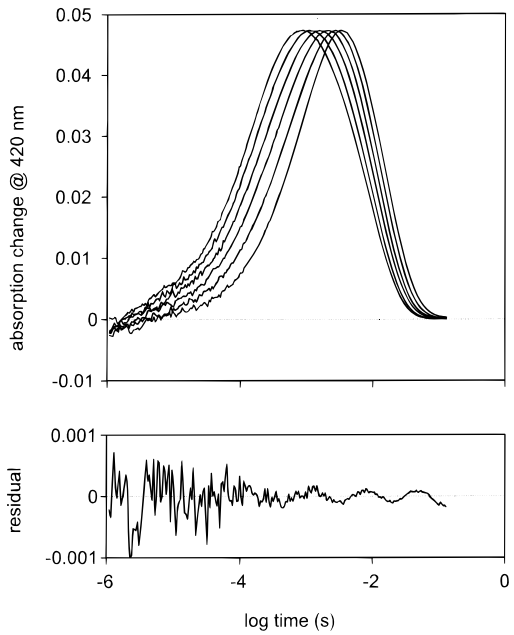

FIGURE 1: Absorption changes at 420 nm after flash photoexcitation of wild-type bacteriorhodopsin in mixtures of H_2O and D_2O. Upper panel: recorded traces at 0, 0.2, 0.4, 0.6, 0.8, and 1.0 mole fraction of D_2O (left to right). The traces are shown with their amplitudes normalized to one another. Lower panel: residual of the fit of the trace with 100% D_2O with three rise and a single decay exponential, on a 10× expanded scale. Conditions: ca. 10 μM bacteriorhodopsin, 0.1 M NaCl, and 10 mM 3-(*N*-morpholino)-2-hydroxypropanesulfonic acid, pH 7.

Deuterium Isotope Effects in Various Site-Specific Mutants. The rise of the M state depends on events that have their

[2] Karpefors, Ädelroth, and Brzezinski, unpublished results.

[3] The magnitude of the standard deviations of the time constants (see Table 1) and a degree of inherent uncertainty in the behavior of proton inventory plots (*27*) allowed us to make only qualitative judgments concerning the shape of these plots. Thus, we describe them as "linear", "somewhat curved", or "greatly curved".

Table 1: Summary of Measured Parameters (Relaxation Time Constant[a] and Amplitude, Kinetic H/D Isotope Effect, and Curvature of Proton Inventory Plot) at 15 °C in Wild-Type Bacteriorhodopsin and the Mutants E204Q, Y57F, R82A, and D96N

protein	step	time, μs[b]	amplitude, %[b]	KIE	curvature
WT	M rise I	3	11	2.1	−
	M rise II	85	32	2.8	+
	M rise III	250	60	5.1	+++
	M decay	9 000	100	1.8	−
E204Q	M rise I	2	24	3.4	−
	M rise II	26	50	5.4	−
	M rise III	60	26	10.4	+++
	M decay I	3 900	28	4.1	+
	M decay II	30 500	72	1.3	−
	O rise	29 400	100	1.1	−
	O decay	153 000	100	5.5	+
Y57F	M rise I	2	30	3.2	−
	M rise II	22	46	6.7	+
	M rise III	70	24	13.1	+++
	M decay	7 600	100	2.1	−
	O rise	13 400	100	1.5	−
	O decay	45 600	100	5.1	−
R82A	M rise I	1	74	3.2	−
	M rise II	5	19	4.3	−
	M rise III	22	7	4.0	−
	M decay I	1 300	14	5.2	−
	M decay II	5 500	61	3.1	−
	M decay III	22 300	25	2.7	−
D96N	M rise I	2	8	1.9	−
	M rise II	40	19	2.4	+
	M rise III	185	33	4.5	++
	M rise IV	810	40	4.2	++

[a] Standard deviations of time constants are approximately 9%, 6%, 1.5%, and 0.5% for M rise I, M rise II, M rise III, and M decay, respectively. [b] Measured in H_2O.

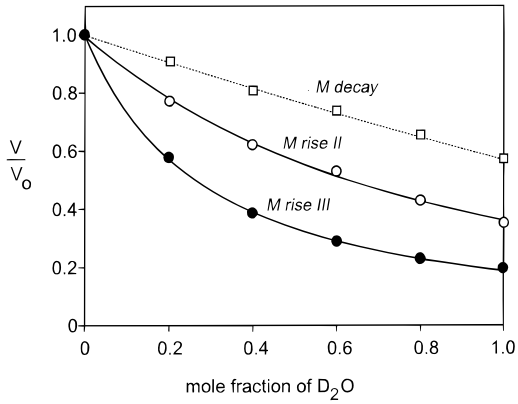

FIGURE 2: Proton inventory plot for the three reactions measurable at 420 nm in the photocycle of wild-type bacteriorhodopsin. The ratio of rates at the indicated mole fraction of D_2O to that in 100% H_2O (V/V_o) is plotted vs the mole fraction of D_2O. Symbols: open circles, second M rise component; closed circles, third M rise component; open squares and dashed line, M decay. Data from Figure 1.

origins mostly in the extracellular region, where numerous residues are critical for proton release: Arg-82 (*33*, *34*), Tyr-57 (*35*), Glu-194 (*36*, *37*), and Glu-204 (*34*). The decay of the M state reflects a proton transfer in the cytoplasmic region, but under some conditions, as in the E204Q mutant at neutral pH, the decay of the O state depends, once again, on proton displacement in the extracellular region (*10*, *11*). Experiments, such as shown in Figures 1 and 2 for the wild-type protein, were done with various mutants containing residue changes in the extracellular region. In some of these mutants the O state accumulated sufficiently to follow its formation and decay by measuring absorption changes at 660 nm.

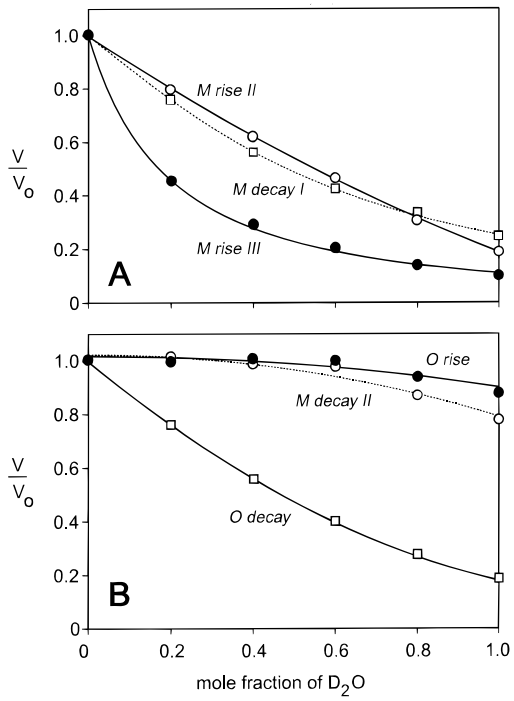

FIGURE 3: Proton inventory plot for four reactions measurable at 420 nm, and two reactions measurable at 660 nm, in the photocycle of E204Q bacteriorhodopsin. The ratio of rates at the indicated mole fraction of D_2O to that in 100% H_2O (V/V_o) is plotted vs the mole fraction of D_2O. Symbols: (A) open circles, second M rise component; closed circles, third M rise component; open squares and dashed line, first M decay component; (B) open circles and dashed line, second M decay component; closed circles, O rise; open squares, O decay. Conditions: as in Figure 1.

Figure 3 shows proton inventory plots for the M and O states of the E204Q mutant. The degrees of curvature for the second and third rise components of the M state (Figure 3A) greatly resemble those of the corresponding processes in the wild-type photocycle (Figure 2). The KIEs for the second and third components were 5.4 and 10.4, respectively (Table 1), which are unusually high values. In this mutant the decay of M was described by a first component with a somewhat greater isotope effect but linear proton inventory plot as in the wild type, and a second with nearly none (Table 1, Figure 3). The time constant of the second decay component was virtually the same as the rise of the O state. Not surprisingly, if the origin of the O rise is the M → O reaction, the O rise exhibited also little if any deuterium isotope effect. On the other hand, the single component of the decay of the O state had a large KIE as found before (*10*, *19*, *22*, *23*), although with only a slight curvature (Figure 3B). Similar experiments were done with the E194Q mutant. Although in this case the best fits of the data did not contain the same number of exponentials at all D_2O concentrations, and that precluded a full analysis, it appeared that the third M rise component exhibited a large KIE and a strongly curved proton inventory plot (not shown), as in E204Q.

The KIEs and the curvature of the proton inventory plots were nearly the same for the Y57F mutant also. As shown in Figure 4, the second and third rise components of M were both strongly affected by D_2O, but only the third component exhibited a strongly curved proton inventory plot (Figure

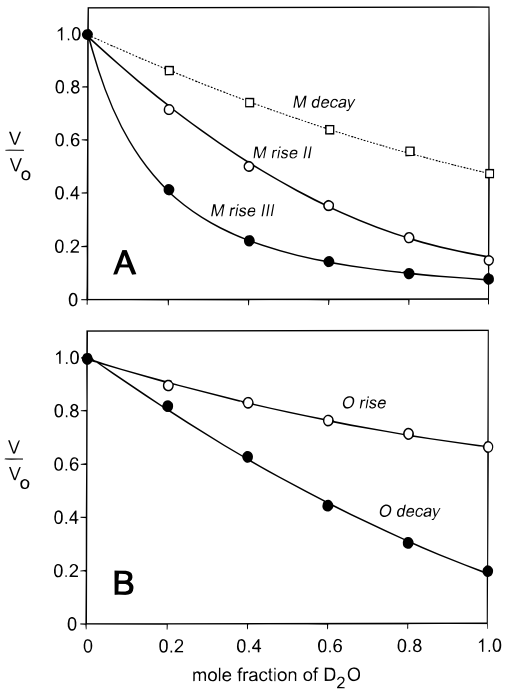

FIGURE 4: Proton inventory plot for three reactions measurable at 420 nm, and two reactions measurable at 660 nm, in the photocycle of Y57F bacteriorhodopsin. The ratio of rates at the indicated mole fraction of D_2O to that in 100% H_2O (V/V_o) is plotted vs the mole fraction of D_2O. Symbols: (A) open circles, second M rise component; closed circles, third M rise component; open squares and dashed line, M decay; (B) open circles, O rise; closed circles, O decay. Conditions: as in Figure 1.

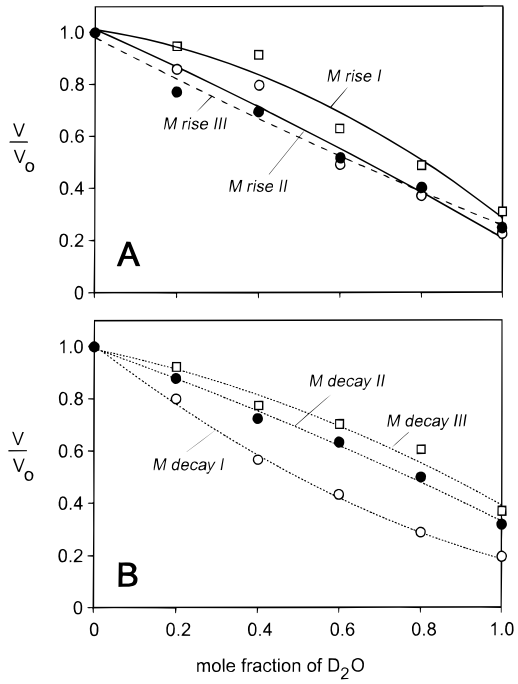

FIGURE 5: Proton inventory plot for six reactions measurable at 420 nm in the photocycle of R82A bacteriorhodopsin. The ratio of rates at the indicated mole fraction of D_2O to that in 100% H_2O (V/V_o) is plotted vs the mole fraction of D_2O. Symbols: (A) open squares, first M rise component; open circles, second M rise component; closed circles, third M rise component; (B) open circles and dashed line, first M decay component; closed circles and dashed line, second M decay component; open squares and dashed line, third M decay component. Conditions: 0.1 M NaCl and 10 mM 3-[(1,1-dimethyl-2-hydroxyethyl)amino]-2-hydroxypropanesulfonic acid, pH 9.

4A). The KIE of the latter was unprecedentedly high (for bacteriorhodopsin), at 13.1 (Table 1). The single decay component of M, which in this case did not coincide with the rise of O because of accumulation of the N state (data not shown), showed a KIE of 2.1 and with a nearly linear plot (Figure 4A, Table 1). The rise of O exhibited very similar deuterium effects to M decay. Decay of the O state, as in E204Q, was strongly affected by D_2O, with a KIE of 5.1 (Table 1), and with only slightly curving proton inventory plot (Figure 4B).

In contrast, the behavior of the R82A mutant was very different from the wide-type protein. As shown in Figure 5A, in this case proton inventory plots could be calculated for all three M rise components, and they were all nearly linear. Importantly, the third rise component of M did not exhibit a curved plot. Less unexpected, the three M decay components observable in this mutant (Figure 5B) showed also little curvature. Because in R82A the pK_a of Asp-85 is about 7 (*38*, *39*), a wild-type-like photocycle is observed only at a pH significantly higher than 7, and the data in Figure 5 were measured at pH 9. A control experiment, with E204Q where proton release during the rise of M is absent (*34*) as in R82A, indicated that its deuterium-dependent behavior is essentially the same at pH 9 (not shown) as at pH 7 (Figure 3). Another control would have been the wild-type protein at high pH where the M rise becomes rapid as in R82A (*40*), but the dependency of the pK_a of this effect on the D_2O/H_2O ratio precluded the use of this system.

The Fourth Rise Component of the M State, Its Deuterium Isotope Effect, and Its Relationship to Proton Release. In the D96N mutant a fourth rise component for M, with a time

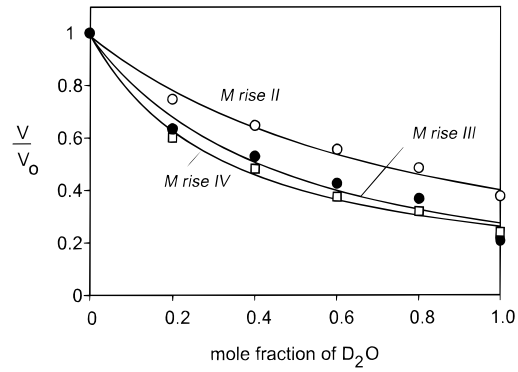

FIGURE 6: Proton inventory plot for the three reactions measurable at 420 nm in the photocycle of D96N bacteriorhodopsin. The ratio of rates at the indicated mole fraction of D_2O to that in 100% H_2O (V/V_o) is plotted vs the mole fraction of D_2O. Symbols: open circles, second M rise component; closed circles, third M rise component; open squares, fourth M rise component. Conditions as in Figure 1 but with 0.4 mM NaN_3.

constant of about 1 ms, was reported (*41*). Although it has large amplitude in this mutant, in the wild-type protein under physiological conditions this transition is not apparent in data around 400 nm and can be seen only in global fits of measurements at other wavelengths (*41*). Figure 6 shows the second, third, and fourth rise components for M rise in D96N. The second and third components behave essentially as in the wild type (Figure 2), and the fourth is seen to exhibit KIE and curved plot similar to the third component.

The phase of M rise identified here as the third component had been kinetically linked to proton release to the extra-

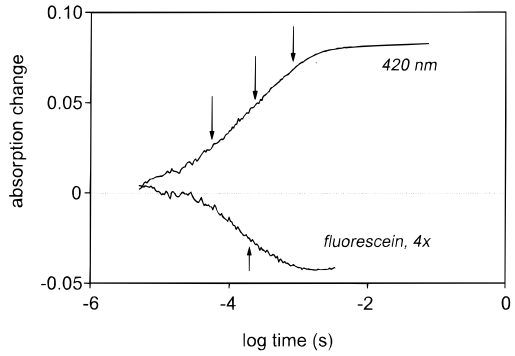

FIGURE 7: Kinetics of M and proton release in the photocycle of D96N bacteriorhodopsin. The measurable relaxation times for the rise of absorption at 420 nm are indicated with downward arrows (55, 230, and 820 μs). The decay of M in this mutant, and at this pH, is too slow to be noticeable on the time scale shown. The trace labeled as fluorescein, 4× was obtained by subtracting a trace measured at 490 nm but in the presence of 20 mM phosphate from the measured trace of D96N bacteriorhodopsin labeled at Lys-129 with fluorescein succinimidyl ester (*43*). Its single relaxation rise time is indicated with an upward arrow (at 190 μs). Conditions: 0.1 M NaCl, pH 7.1.

cellular surface (*42*), although under some conditions this linkage was found to be not strict (*21*). We have reexamined this question in the D96N mutant where a fourth component is also measurable, and data on proton release has not been reported. Figure 7 shows that, consistent with results with the wild-type protein, the time course of proton release in D96N is nearly the same as, although not identical to, the third rise component of the M rise. The kinetics of M and proton release, followed with fluorescein covalently bound to Lys-129, located on the extracellular surface (*21, 43*), are shown in Figure 7. The absorption change of the pH indicator dye is described by a single exponential, with a time constant of 190 μs, while the time constant of the third M rise component is 230 μs, both indicated by arrows.

DISCUSSION

We find that the consequences of replacing H_2O with D_2O on the photocycle reactions of bacteriorhodopsin, which include the KIE of the relaxation rates and the degree of curvature of proton inventory plots, are greatly diverse. However, the patterns we observe are self-consistent in the wild-type protein and selected mutants and allow some conclusions to be made of the molecular events that limit the reactions. From what is known about proton conduction from theory (*44*) and other proteins studied (*27*), three basic kinds of deuterium effects can be distinguished: (i) Reactions with relatively small ($\leq 2\times$) KIE and linear proton inventory plots. This behavior originates from proton transfers limited by hydrogen bond breaking or hydrogen bond reorientation (e.g., between water molecules). (ii) Reactions with large KIE (up to 10×) and strongly curved (e.g., quadratic) proton inventory plots. This behavior originates from complex, multiproton transfer events, with the nonlinearity arising from cooperativity in the transition state. Distinguishing these from simple proton transfers is the primary goal of using the proton inventory method (*27*). (iii) Reactions with large ($6-10\times$) KIE but linear proton inventory plots. This behavior originates from simple proton transfers if they are limited by proton hopping between two heavy atoms with similar proton affinities (*44*).

The interpretation of the observed deuterium effects in such mechanistic terms is relatively simple when the parameters examined are rate constants. Rate constants can be calculated for a complex reaction sequence like the bacteriorhodopsin photocycle also, but they are model-dependent, and the fits of the data to the available models have not been good enough so far to decide the kinds of subtle differences required in these evaluations. For this reason, we used relaxation rates whose values are determined directly by fitting the data to sums of exponentials. They will depend, at least in principle, on several individual rate constants. If the rate constants whose combination determines the relaxation in question have different KIEs, the shapes of proton inventory plot for the relaxation rate may be misleading because they could show curvature for this reason alone. However, this is unlikely to be so for the single case of strong curvature we found. The observation of uniquely high KIE for the third (and fourth) rise component of M in its time domain implies that a single rate constant dominates the expression that defines its rate. Another possible source of error would be if the D^+/H^+ equilibration were slower than the rates of the photocycle reactions measured, as it would split each time constant into two, from the protonated and the deuterated species. Indeed, such equilibration of the Schiff base with the medium occurs in a few milliseconds (*45*), which is longer than the M rise components measured. However, the observation that the number of exponentials at the various D_2O/H_2O ratios remained unchanged indicates that there is rapid exchange of D^+ and H^+, probably among groups within the protein.

The structure of the extracellular region (*25, 26*), where the investigated deuterium isotope effects on M rise and O decay will arise, is shown, from two viewing angles for clarity, in Figure 8. Water 402 at the active center accepts a hydrogen bond from the Schiff base and donates hydrogen bonds to the anionic Asp-85 and Asp-212. Asp-212 is firmly stabilized as an anion by hydrogen bonds with the phenolic hydroxyls of Tyr-57 and Tyr-185. Asp-85, on the other hand, is hydrogen-bonded to the potentially more mobile Thr-89 and water 401. A three-dimensional extended hydrogen-bonded network connects the Schiff base region with the extracellular surface. Two pairs of hydrogen-bonded water molecules, waters 401 and 406, and waters 403 and 404, flank the guanidinium group of Arg-82 (numbering of water molecules from ref *25*). This geometry is further stabilized by water 407 that bridges Tyr-57 and Arg-82. Water 404 connects with Glu-194, which is hydrogen-bonded to Glu-204 near the extracellular surface. The deuterium effects are discussed below in terms of this structure.

First and Second Components of M Rise. Absorption changes at 420 nm originate nearly entirely from changes in the protonated state of the Schiff base. Although in this sense all phases of M rise measure the deprotonation of the retinal Schiff base, in the kinetic model we use (*8, 9, 12*) the first rise component occurs with the time constant of the K ↔ L equilibration, which corresponds to a relaxation of the retinal chain (*46*), and rearrangements of bound water and some side chains in the protein (reviewed in ref *47*). This component was readily measurable only in R82A, where its KIE was 3.1, and its proton inventory plot was nearly linear. The second component occurs with the time constant of the L ↔ M_1 reaction, i.e., the establishment of a

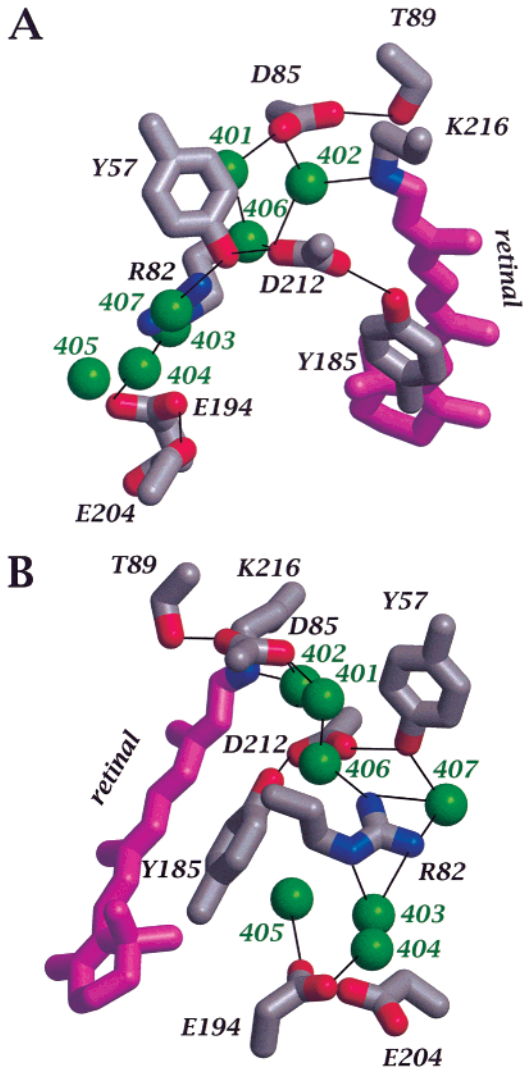

FIGURE 8: Two views of the extracellular region of bacteriorhodopsin at different angles, from X-ray diffraction (*25*). View A shows water 402 which, is hydrogen-bonded to the retinal Schiff base and to Asp-85 and Asp-212, and the additional hydrogen bonds of the two aspartic acid side chains. View B shows the hydrogen bonds of Arg-82 to water molecules 406 and 407 on one hand and to water molecules 403 and 404 on the other, as well as the relationship of Glu-194 and Glu-204 to the latter two water molecules.

protonation equilibrium between Asp-85 and the Schiff base. Its relaxation rate contains the forward and reverse rate constants for this equilibration and, depending on the exact details of the model, to a lesser extent also the rate constants of the preceding and the following reactions. This component shows widely varying KIEs of 2.4−6.7, in the wild type and in different mutants, but always only a small curvature in the proton inventory plot. We conclude that the rate of the protonation of Asp-85 by the Schiff base is limited by a simple proton transfer step but one that is affected by residues of the extracellular network. The simplest model would be proton transfer through the hydrogen bonds of water 402 that bridges the donor and the acceptor (Figure 8A). However, on purely geometrical grounds it might be expected that isomerization of the retinal from the all-*trans* configuration in Figure 8 to the 13-*cis*,15-*anti* in the L state will have moved the Schiff base N−H bond away from water 402, as indeed observed later in the photocycle, in the M state (*26*). If this rotation of the retinylidene nitrogen in L is only partial, e.g., because of Coulombic interaction between the anionic Asp-85 and the positively charged protonated Schiff base, a direct proton transfer might be still possible. If the rotation is complete in the L state, however, the protonation of Asp-85 must be a more complex process, one that might involve removing a hydroxyl ion from water 402. The latter is an interesting possibility because it could be analogous to chloride ion transfer at this location in the photocycle of the halorhodopsin (*48*, *49*) and the D85T mutant of bacteriorhodopsin (*50*, *51*).

Third Component of M Rise. In the kinetic model we use here, this phase represents a shift of the protonation equilibrium between Asp-85 and the Schiff base toward further proton transfer to Asp-85. It is more or less coincident with proton release to the extracellular surface, which originates from dissociation of a site that was suggested to be Glu-204 (*34*), the Glu-194 and Glu-204 pair (*52*), a water bound in this region (*53*), or a hydrogen-bonded continuum (*54*). Coupling of the protonation of Asp-85 and the proton release was suggested from the anomalous titration behavior of Asp-85 (*5*, *33*) and the absence of the titration anomaly in all mutants where proton release was absent (*6*, *36*, *55*). Consistent with the model, in these mutants, as well as at pH well below the pK_a for proton release, the normal amplitude of M is not reached (*8*, *9*), and the persistence of the L ↔ M_1 equilibrium is indicated by the continued presence of the L state (*56*, *57*). Recent structural information provides a molecular rationale for this model. The displacement of the side chain of Arg-82 observed in the late M state (*26*) makes it likely that the proton release is coupled to the protonation of Asp-85 through the shuttling of the positively charged guanidinium group between the inward and outward directions. This suggests that the released proton originates from the vicinity of the two glutamic acid residues (Figure 8).

The KIE of the third rise component is as large as 5−13, and the proton inventory plot is strongly curved, suggesting that this process is linked to several simultaneous proton transfers or on simultaneously breaking (or making) several hydrogen bonds. These events do not depend on the specific hydrogen-bonding geometry of Glu-204 (and Glu-194) or Tyr-57 because replacing these residues with glutamine and phenylalanine, respectively, does not decrease the deuterium effects for the third M rise component (Table 1, Figures 3A and 4A). Interestingly, in these mutants the KIE is much greater than in the wild type (Table 1), indicating that, although its nature is unchanged, the process is affected by the residue replacements. On the other hand, the complexity of the events in the transition does depend on Arg-82, because both the large KIE and the curvature disappear in the R82A mutant (Table 1, Figure 5A). These findings seem to rule out water molecules 407 and 405, and probably 403 and 404, and implicate water molecules 401, 402, and 406 between the Arg-82 side chain and Asp-85 (Figure 8). It appears that when the guanidinium group is removed, as in the R82A mutant, part of the process that occurs after the initial proton equilibration between the Schiff base and Asp-85 is retained but the observed much simpler deuterium effect suggests that it is no longer a multiproton reaction. Unlike in the wild-type protein, this changed reaction is not connected to proton release during the formation of M (*58*).

Presumably, therefore, the observed deuterium effects originate not from the proton release but from events near Arg-82 (and therefore Asp-85 and the Schiff base) that give rise to it. Proximity of the changes during the last rise component of M to the Schiff base was suspected from the earlier observation of a blue shift in the maximum of the M state of D96N mutants (*8, 21*), coincident with the last M rise component (*59*).

Fourth Component of M Rise. Its time constant places this kinetic component, that shifts the protonation equilibrium further to deprotonation of the Schiff base, well after proton release (Figure 7). The large deuterium isotope effect and the strong curvature of the proton inventory plot (Figure 6) indicate that the transition depends on a complex process, similarly to the third component. It is not clear whether this is the result of a dependence of this transition on the rate constant in the third M rise component or a conformational change in the $M_1 \rightarrow M_2$ reaction sequence with its own, independent, complexity. Neither is it clear why this transition, found as an unspecified relaxation in the wild-type photocycle (*41*), appears as a major component of the M rise kinetics in the D96N mutant.

Decay of the M State. The decay of the M intermediate reflects reprotonation of the Schiff base, either from Asp-96 (in the wild type) or from the cytoplasmic surface (in Asp-96 mutants). Under various conditions, and in various mutants, this transition is resolved into one, two, or three kinetic components. The interpretation of multiple decay components has been much disputed, but there is evidence to support the model in which these components originate from M ↔ N (*14, 15, 60, 61*) and N ↔ O (*62*) equilibration reactions. In the cases examined in the present study, the deuterium effects on these kinetic components were small to moderate, with little if any curvature in the proton inventory plots. Thus, it appears that the rates of proton transfer to the Schiff base and the reactions which immediately follow it are limited by simple proton transfer. One exception is the second M decay component of the E204Q photocycle, which is nearly unaffected by deuterium replacement (Figure 3B). Its rate, coincident with the rise of O, is likely to depend on the reisomerization of the retinal to all-*trans*, because the O state is the first one in the photocycle to contain all-*trans*-retinal (*63*). Another exception is the first M decay component of the R82A photocycle, which exhibits a large deuterium isotope effect, although with little curvature (Figure 5B). The reason for this is unclear.

The KIE of M decay was studied in the photocycles of the D96N and D96G mutants (*64*). Its value was 1.2−4.7 and was strongly dependent on pH (higher at lower pH) between 4 and 8. The latter suggested that the rate-limiting step is different at low pH and that this might have to do with an internal proton donor to the Schiff base in the Asp-96 mutants, other than Asp-96 (*64*). The structure of the protein provides no clues to what this group might be.

Rise and Decay of the O State. In the rise of the O intermediate the retinal is reisomerized to a twisted all-*trans* configuration (*62, 65*). Its decay includes relaxation of the polyene chain. However, the similarity of the effects of various residue replacements on the O decay rate and the deprotonation rate of Asp-85 by pH jump in the unphotolyzed protein suggested (*10*) that, at least in the case of mutants with slow decay, it is limited by the proton transfer from Asp-85, either directly to the surface (at pH < pK_a for release) or to the still vacant extracellular proton release site (at pH > pK_a for release). In the cases where O accumulates, in the E204Q and Y57F mutants (Figures 3 and 4) as well as in E194Q (not shown), both rise and decay are described by single exponentials. The rise is very little affected by D_2O replacement, as expected if it is limited primarily by the rate of isomerization rather than a proton transfer step. The decay exhibits very large KIE, as found before (*10, 19, 22, 23*), but the proton inventory plots show only minor curvature (Figures 3B and 4B). Deprotonation of Asp-85 is therefore limited by a single proton transfer process, which has deuterium isotope effects characteristic of proton hopping. Recently, the transient protonation of a carboxyl group during O decay, linked kinetically to deprotonation of Asp-85, was reported (*66*). The ^{13}C isotope shifts of the COOH and COO^- bands suggested that it is the carboxyl group of Asp-212. An attractive possibility is that this residue, located near Asp-85 (Figure 8), is the immediate proton acceptor to Asp-85, and that this proton transfer is the limiting step in the decay of O. Thus, although both reactions exhibit very high KIEs and take place in the same region of the protein, the deprotonation of Asp-85 in O decay is unlike the protonation of Asp-85 earlier in the cycle, whose major (third) component appears to be limited by a concerted reaction that has deuterium isotope effects characteristic of cooperative hydrogen bond reorientation.

ACKNOWLEDGMENT

Valuable discussions with Peter Brzezinski are gratefully acknowledged.

REFERENCES

1. Lanyi, J. K. (1993) *Biochim. Biophys. Acta 1183*, 241−261.
2. Lanyi, J. K. (1998) *J. Struct. Biol. 124*, 164−178.
3. Oesterhelt, D. (1998) *Curr. Opin. Struct. Biol. 8*, 489−500.
4. Haupts, U., Tittor, J., and Oesterhelt, D. (1999) *Annu. Rev. Biophys. Biomol. Struct. 28*, 367−399.
5. Balashov, S. P., Imasheva, E. S., Govindjee, R., and Ebrey, T. G. (1996) *Biophys. J. 70*, 473−481.
6. Richter, H. T., Brown, L. S., Needleman, R., and Lanyi, J. K. (1996) *Biochemistry 35*, 4054−4062.
7. Govindjee, R., Misra, S., Balashov, S. P., Ebrey, T. G., Crouch, R. K., and Menick, D. R. (1996) *Biophys. J. 71*, 1011−1023.
8. Váró, G., and Lanyi, J. K. (1991) *Biochemistry 30*, 5008−5015.
9. Zimányi, L., Váró, G., Chang, M., Ni, B., Needleman, R., and Lanyi, J. K. (1992) *Biochemistry 31*, 8535−8543.
10. Richter, H. T., Needleman, R., Kandori, H., Maeda, A., and Lanyi, J. K. (1996) *Biochemistry 35*, 15461−15466.
11. Balashov, S. P., Lu, M., Imasheva, E. S., Govindjee, R., Ebrey, T. G., Othersen, B. I., Chen, Y., Crouch, R. K., and Menick, D. R. (1999) *Biochemistry 38*, 2026−2039.
12. Váró, G., Lanyi, J. K. (1991) *Biochemistry 30*, 5016−5022.
13. Ludmann, K., Gergely, C., and Váró, G. (1998) *Biophys. J. 75*, 3110−3119.
14. Zimányi, L., Cao, Y., Needleman, R., Ottolenghi, M., and Lanyi, J. K. (1993) *Biochemistry 32*, 7669−7678.
15. Druckmann, S., Heyn, M. P., Lanyi, J. K., Ottolenghi, M., and Zimányi, L. (1993) *Biophys. J. 65*, 1231−1234.
16. Eisfeld, W., Pusch, C., Diller, R., Lohrmann, R., and Stockburger, M. (1993) *Biochemistry 32*, 7196−7215.
17. Bitting, H. C., Jang, D.-J., and El-Sayed, M. A. (1990) *Photochem. Photobiol. 51*, 593−598.
18. Shrager, R. I., Hendler, R. W., and Bose, S. (1995) *Eur. J. Biochem. 229*, 589−595.

19. Korenstein, R., Sherman, W. V., and Caplan, S. R. (1976) *Biophys. Struct. Mech. 2*, 267−276.
20. Liu, S. Y. (1990) *Biophys. J. 57*, 943−950.
21. Cao, Y., Brown, L. S., Sasaki, J., Maeda, A., Needleman, R., and Lanyi, J. K. (1995) *Biophys. J. 68*, 1518−1530.
22. Le Coutre, J., and Gerwert, K. (1996) *FEBS Lett. 398*, 333−336.
23. Mantele, W., Siebert, F., and Kreutz, W. (1981) *FEBS Lett. 128*, 249−254.
24. Berlhali, H., Nollert, P., Royant, A., Menzel, C., Rosenbusch, J., Landau, E. M., and Pebay-Peyroula, E. (1999) *Structure 7*, 909−917.
25. Luecke, H., Schobert, B., Richter, H. T., Cartailler, J.-P., and Lanyi, J. K. (1999) *J. Mol. Biol. 291*, 899−911.
26. Luecke, H., Schobert, B., Richter, H. T., Cartailler, J.-P., and Lanyi, J. K. (1999) *Science 286*, 255−260.
27. Venkatasubban, K. S., and Schowen, R. L. (1982) *CRC Crit. Rev. Biochem. 17*, 1−44.
28. Oesterhelt, D., and Stoeckenius, W. (1974) *Methods Enzymol. 31*, 667−678.
29. Needleman, R., Chang, M., Ni, B., Váró, G., Fornes, J., White, S. H., and Lanyi, J. K. (1991) *J. Biol. Chem. 266*, 11478−11484.
30. Brown, L. S., Needleman, R., and Lanyi, J. K. (1999) *Biochemistry 38*, 6855−6861.
31. Covington, A. K., Paabo, M., Robinson, R. A., and Bates, R. G. (1968) *Anal. Biochem. 40*, 700−706.
32. Zimányi, L., Kulcsár, A., Lanyi, J. K., Sears, D. F., Jr., and Saltiel, J. (1999) *Proc. Natl. Acad. Sci. U.S.A. 96*, 4414−4419.
33. Balashov, S. P., Govindjee, R., Imasheva, E. S., Misra, S., Ebrey, T. G., Feng, Y., Crouch, R. K., and Menick, D. R. (1995) *Biochemistry 34*, 8820−8834.
34. Brown, L. S., Sasaki, J., Kandori, H., Maeda, A., Needleman, R., and Lanyi, J. K. (1995) *J. Biol. Chem. 270*, 27122−27126.
35. Govindjee, R., Kono, M., Balashov, S. P., Imasheva, E., Sheves, M., and Ebrey, T. G. (1995) *Biochemistry 34*, 4828−4838.
36. Balashov, S. P., Imasheva, E. S., Ebrey, T. G., Chen, N., Menick, D. R., and Crouch, R. K. (1997) *Biochemistry 36*, 8671−8676.
37. Dioumaev, A. K., Richter, H. T., Brown, L. S., Tanio, M., Tuzi, S., Saitô, H., Kimura, Y., Needleman, R., and Lanyi, J. K. (1998) *Biochemistry 37*, 2496−2506.
38. Otto, H., Marti, T., Holz, M., Mogi, T., Stern, L. J., Engel, F., Khorana, H. G., and Heyn, M. P. (1990) *Proc. Natl. Acad. Sci. U.S.A. 87*, 1018−1022.
39. Brown, L. S., Bonet, L., Needleman, R., and Lanyi, J. K. (1993) *Biophys. J. 65*, 124−130.
40. Balashov, S. P., Govindjee, R., and Ebrey, T. G. (1991) *Biophys. J. 60*, 475−490.
41. Drachev, L. A., Kaulen, A. D., and Komrakov, A. Y. (1992) *FEBS Lett. 313*, 248−250.
42. Alexiev, U., Marti, T., Heyn, M. P., Khorana, H. G., and Scherrer, P. (1994) *Biochemistry 33*, 13693−13699.
43. Heberle, J., and Dencher, N. A. (1992) *Proc. Natl. Acad. Sci. U.S.A. 89*, 5996−6000.
44. Agmon, N. (1995) *Chem. Phys. Lett. 244*, 456−462.
45. Deng, H., Huang, L., Callender, R., and Ebrey, T. G. (1994) *Biophys. J. 66*, 1129−1136.
46. Braiman, M. S., and Mathies, R. A. (1982) *Proc. Natl. Acad. Sci. U.S.A. 79*, 403−407.
47. Maeda, A., Kandori, H., Yamazaki, Y., Nishimura, S., Hatanaka, M., Chon, Y. S., Sasaki, J., Needleman, R., and Lanyi, J. K. (1997) *J. Biochem. (Tokyo) 121*, 399−406.
48. Váró, G., Needleman, R., and Lanyi, J. K. (1995) *Biochemistry 34*, 14500−14507.
49. Rüdiger, M., and Oesterhelt, D. (1997) *EMBO J. 16*, 3813−3821.
50. Sasaki, J., Brown, L. S., Chon, Y.-S., Kandori, H., Maeda, A., Needleman, R., and Lanyi, J. K. (1995) *Science 269*, 73−75.
51. Tittor, J., Haupts, U., Haupts, C., Oesterhelt, D., Becker, A., and Bamberg, E. (1997) *J. Mol. Biol. 271*, 405−416.
52. Essen, L. O., Siegert, R., Lehmann, W. D., and Oesterhelt, D. (1998) *Proc. Natl. Acad. Sci. U.S.A. 95*, 11673−11678.
53. Luecke, H., Richter, H. T., and Lanyi, J. K. (1998) *Science 280*, 1934−1937.
54. Rammelsberg, R., Huhn, G., Lübben, M., and Gerwert, K. (1998) *Biochemistry 37*, 5001−5009.
55. Richter, H. T., Needleman, R., and Lanyi, J. K. (1996) *Biophys. J. 71*, 3392−3398.
56. Althaus, T., and Stockburger, M. (1998) *Biochemistry 37*, 2807−2817.
57. Brown, L. S., Dioumaev, A. K., Needleman, R., and Lanyi, J. K. (1998) *Biophys. J. 75*, 1455−1465.
58. Balashov, S. P., Govindjee, R., Kono, M., Imasheva, E., Lukashev, E., Ebrey, T. G., Crouch, R. K., Menick, D. R., and Feng, Y. (1993) *Biochemistry 32*, 10331−10343.
59. Drachev, L. A., Kaulen, A. D., and Komrakov, A. Y. (1993) *Biochem. Int. 30*, 461−469.
60. Otto, H., Marti, T., Holz, M., Mogi, T., Lindau, M., Khorana, H. G., and Heyn, M. P. (1989) *Proc. Natl. Acad. Sci. U.S.A. 86*, 9228−9232.
61. Ames, J. B., and Mathies, R. A. (1990) *Biochemistry 29*, 7181−7190.
62. Chernavskii, D. S., Chizhov, I. V., Lozier, R. H., Murina, T. M., Prokhorov, A. M., and Zubov, B. V. (1989) *Photochem. Photobiol. 49*, 649−653.
63. Smith, S. O., Pardoen, J. A., Mulder, P. P. J., Curry, B., Lugtenburg, J., and Mathies, R. A. (1983) *Biochemistry 22*, 6141−6148.
64. Miller, A., and Oesterhelt, D. (1990) *Biochim. Biophys. Acta 1020*, 57−64.
65. Kandori, H., Yamazaki, Y., Hatanaka, M., Needleman, R., Brown, L. S., Richter, H. T., Lanyi, J. K., and Maeda, A. (1997) *Biochemistry 36*, 5134−5141.
66. Dioumaev, A. K., Brown, L. S., Needleman, R., and Lanyi, J. K. (1999) *Biochemistry 38*, 10070−10078.

BI9921900